lajss.org
Latin American Journal of Solids and Structures
www.lajss.org

Modeling of masonry shear walls subjected to in-plane lateral loads using frame elements with variable cross-sections

Rodrigo Bird Burgos[a*] 0000-0003-0326-395X, Aline dos Santos Alves Gesteira[b], Maria Fernanda Figueiredo de Oliveira[a] 0000-0001-5359-7523, Lucas Encarnação Silva[a] 0000-0002-7756-5320

[a] Rio de Janeiro State University (UERJ), Rio de Janeiro, RJ, Brazil. Email: rburgos@eng.uerj.br, mariafer@eng.uer.br, lucas.encarnacao21@gmail.com
[b] Pontifical Catholic University of Rio de Janeiro (PUC-Rio), Rio de Janeiro, RJ, Brazil. Email: alinegesteira20@gmail.com

* Corresponding author

Abstract
A simple way to obtain numerically the lateral load capacity curve of a masonry wall is to consider it as a one-dimensional element and perform a finite element incremental analysis. Based on some assumptions concerning the normal stress distribution, the panel can be discretized into frame elements whose geometrical properties are evaluated from the portion of the cross-section subjected to compression. In the case of employing finite elements of constant cross-sections, satisfactory results are obtained only if the mesh is dense enough to accurately represent the change in the geometrical properties of the resisting portion of the panel cross-section. In this work, a finite element with a variable cross-section is employed, so the number of elements required for a reliable solution can be reduced. The proposed model is tested against some experimental results available in the literature. Results are in good agreement with reference curves, showing that the proposed model may be employed to assess the load capacity of masonry shear walls in a pre-design phase.

Keywords
Lateral load capacity, variable cross-section, masonry shear wall, frame finite element.

1 INTRODUCTION

Masonry constructions make up an important part of buildings in the world and represent a singular cultural heritage for many countries. It consists of an anisotropic composite material with asymmetry in tension and compression, high nonlinearity in compression, and near-fragile rupture. Despite having a complex mechanical behavior, which makes numerical modeling difficult (Gürel et al., 2006), it is widely used due to its high compressive strength, ease of implementation and material availability, low maintenance cost, durability, and good sound and fire protection (Lu et al., 2005).

It is interesting to point out that, despite the relevance of axial loads in the design of masonry buildings, the deformation capacity of the whole structure under lateral load is required to assess its response to natural events such as winds or earthquakes (Gürel et al., 2012). In this sense, an in-plane pushover/cyclic analysis may be performed by macro-element modeling, in which each masonry wall is idealized as a set of piers and spandrels that are discretized into appropriate nonlinear three-dimensional elements (Asikoglu et al., 2020). In this approach, discrete models of large masonry structures may be built and simulated with time and computational efficiency (Roca et al., 2010, and Lourenço, 2013), while reasonably describing the shear and flexural response.

In the case of peers, the nonlinear frame elements employed should be able to simulate the following failure mechanisms of masonry panels due to lateral loads: flexural (rocking) failure, diagonal crack shear failure, and shear sliding failure (Salmanpour et al., 2013). For this purpose, several elements have been proposed in literature: equivalent beam-based elements to be applied in the equivalent frame model (Roca et al., 2005), and elements with nonlinear spring elements, as described in D'Altri et al. (2020).

Galasco et al. (2004) and Lagomarsino et al. (2013) implemented in the TREMURI program a macro-element that considers the shear-sliding damage evolution by means of internal variables and makes use of ultimate shear and bending strength values from analytical expressions. Later, this macro-element has been refined in the failure models for the use in cyclic analysis by Penna et al. (2014). In addition, Penna et al. (2015) included second-order effects in the formulation. Sabatino and Rizzano (2010) developed the software FREMA with the spread plasticity approach, in which structural elements are discretized into several slices that are modeled in terms of moment-rotation and shear-displacement curves. Addessi et al. (2014) and Liberatore and Addessi (2015) formulated a macro-element with no tension and a lumped nonlinear shear arranged in series. Raka et al. (2015) employed nonlinear constitutive laws at the fiber section level with bending and axial responses decoupled from shear response to propose a fiber element in a force-based formulation.

Since only a few computational programs include these specialized elements for masonry structural modeling, recently many studies have been carried out in literature on the viability of using commercial finite element programs that are adopted by practicing engineers (Salonikios et al., 2003, Pasticier et al., 2008, and Petrovcic and Kilar, 2013). In these studies, shear capacity curves and critical shear values of each masonry panel are employed to evaluate constitutive relations of lumped plastic hinges. In this sense, the lateral load versus displacement curve for each comprising wall under a certain normal load provides essential information for modeling the structure's overall behavior (Salmanpour et al., 2013).

As pointed out in Simões et al. (2015), in addition to the global in-plane behavior assessed by means of macro-element modeling, the out-of-plane response of individual elements should be addressed for a complete assessment of the building response to lateral loads. The work of Mura (2008) presents the analytical expressions of each equilibrated stress state of a panel section under combined load for the stability analysis comprehensively. A good review on beam elements for modeling stability may be found in Addessi et al. (2020).

In literature, several studies on analytical shear limits and capacity curves have been conducted, such as the pioneer works of Heyman (1966) and Di Pasquale (1992), who presented useful solutions for unreinforced masonry under the assumptions that the material does not withstand tensile stresses, and the compression response has perfect elastoplastic behavior. Magenes and Calvi (1997) and Roca (2006) developed a simple and efficient equilibrium model for determining the ultimate load-carrying capacity of masonry shear walls. Benedetti and Steli (2008) improved the analytical response curves by satisfying the axis-wise equilibrium conditions. Three states of normal stress distribution are considered: fully elastic, cracked elastic, and elastic-plastic, by assuming a no-tension and elastic-plastic behavior in compression constitutive law. Displacements and rotations are obtained by integration of the curvature diagram in each equilibrium configuration of the masonry panel under compression and shear.

Similarly, under the same constitutive laws for masonry, Grande et al. (2013) proposed a simple approach to obtain the capacity curve of panels by means of a nonlinear finite element analysis. For each lateral load increment, the masonry panel is divided according to the normal stress state, and each segment is discretized into a one-dimensional frame element, which considers both bending and shear deformation (Timoshenko beam theory), considering a constant cross-

section. Geometrical properties are evaluated from the portion of the cross-section subjected to compression and averaged along each segment. This approach was validated numerically and tested against experimental results for masonry shear panels with and without reinforcements. Although a mesh of only one to three elements has been used in the examples, an investigation on mesh refinement performed in the present study shows that more elements might be required for achieving accurate results.

This work proposes a modification to Grande et al. (2013) by employing a Timoshenko frame finite element with variable cross-section by taking the width as varying linearly along the axis (Gesteira et al., 2020). Therefore, geometrical properties are better approximated along each segment and exactly evaluated at nodal extremities. As a result, the number of elements required for an accurate solution can be reduced, since the compressed portion of the cross-section along the masonry panel is better represented. Although the present formulation is derived for unreinforced masonry, it may be easily adapted to include reinforcements. It should be noticed that this formulation disregards the sliding along bed mortars, and it is appropriate to simulate the panel displacement curve under flexural/rocking failure, similarly to the approach presented in Grande et al. (2013). In addition, a homogenized isotropic behavior is assumed for the masonry composite material, in which stresses at units and mortars are taken in an average manner, a common practice in macro-element modeling.

2 MASONRY SHEAR WALL BEHAVIOR

This work proposes a one-dimensional analysis of a masonry panel through the Finite Element Method (FEM). In this context, Grande et al. (2013) approach is investigated and improved by using finite elements with variable cross-sections and by discretizing the segments with variable width using more than one constant cross-section finite element. In this study, the masonry is considered as a homogeneous material, i.e., endowed with average elastic properties, which were obtained by laboratory tests. It is assumed that the masonry does not withstand tensile stresses and the compression response follows a perfect elastoplastic behavior, i.e., the masonry compressive strength f_{mk} is never exceeded. When f_{mk} is reached, it is kept constant and any additional deformation is exclusively of a plastic nature, between limit elastic strain ε_y and ultimate strain ε_u, as depicted in Fig 1. The modulus of elasticity E is the slope of the elastic portion of the curve and can be obtained by the ratio between f_{mk} and ε_y, i.e., $E = f_{mk}/\varepsilon_y$.

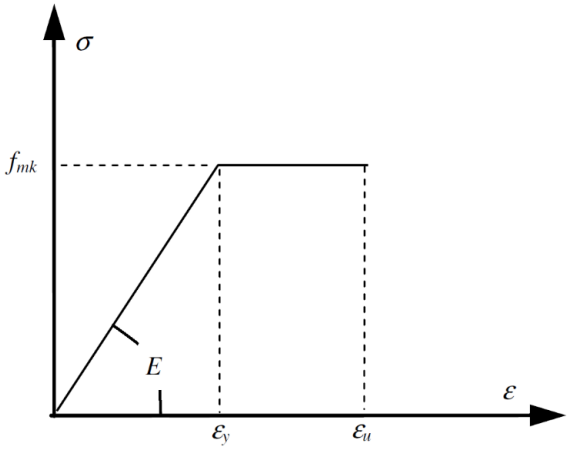

Figure 1 Stress-strain curve used in this study.

As shown in Fig 2, for a lateral force value V, the panel with height H, width B, and depth t can be considered as composed of different segments along the structure height. Thus, each section has a characteristic stress-strain state and a certain height. The number of segments and their extensions depend on parameters such as the masonry properties, the applied load value, and the geometry of the panel. Adopting $\varepsilon_{máx}$ as the maximum strain value when the material is subjected to compression, ε_y as the limit elastic strain value for the masonry, and x as the position of the neutral axis at the base of the panel, the following segments can be determined as:

(a) Segment 1: Whole cross-section is compressed $(x \geq B)$, the material is in the elastic state $(\varepsilon_{máx} \leq \varepsilon_y)$;

(b) Segment 2: Part of the cross-section is compressed $(x < B)$, the material remains in the elastic state $(\varepsilon_{máx} \leq \varepsilon_y)$;

(c) Segment 3: Part of the cross-section is compressed $(x < B)$, but the material behaves in the plastic state $(\varepsilon_{máx} > \varepsilon_y)$.

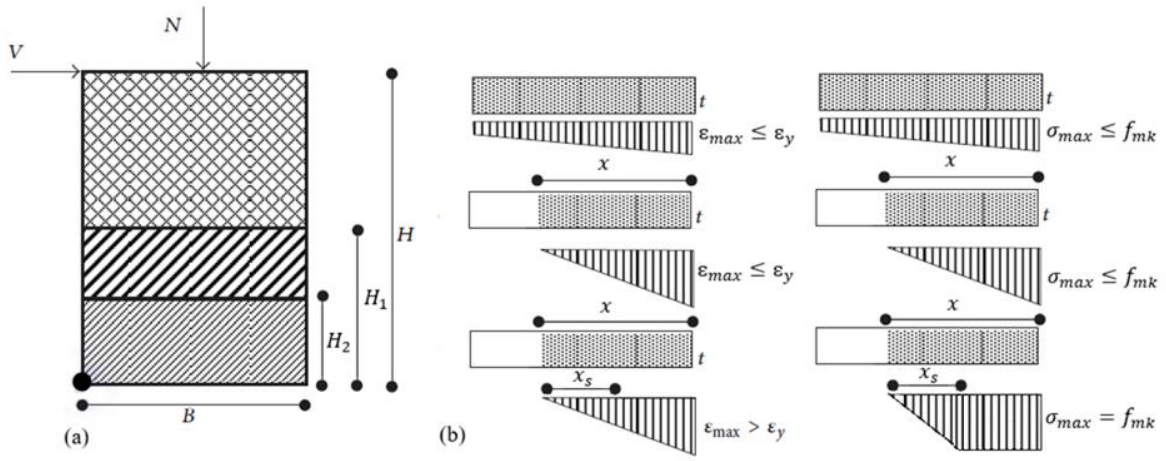

Figure 2 (a) Three-zone masonry panel and (b) corresponding stress-strain states (adapted from Grande et al., 2013).

The lateral load curve vs. lateral deflection at the top of the panel (*V* vs. *D*) is obtained by an incremental nonlinear analysis. Each curve point is determined in two steps. First, for a lateral force value *V*, the number of segments in the panel is determined, as are the corresponding stress-strain states. Then, the displacement *D* is calculated by the finite element method. In this work, the second step is performed in three different ways. The first stage is the reproduction of the numeric analysis used by Grande et al. (2013), i.e., discretization of one constant cross-section finite element to calculate displacement using the Finite Element Method. In this case, the width of the constant cross-section is obtained by the average of the segment's top and bottom values. The second way consists of discretizing the model into 10 constant cross-section finite elements per segment. The number of elements (10) was reached after performing a mesh study, as shown in section 3. Finally, the third way consists of discretizing each segment using one finite element with a variable cross-section. The formulations were implemented in MATLAB (MathWorks, 2018) and assessed on examples obtained in the literature. Considering all the limitations that arise from modeling an orthotropic 2D structure using one-dimensional frame elements, the main contribution of this study is the possibility of performing a finite element analysis with minimal discretization. For this task, this work takes advantage of the implementation of a variable cross-section finite element, whose stiffness coefficients come from the analytical expressions for this condition.

3 PANEL CROSS-SECTION EQUILIBRIUM

From panel cross-section equilibrium at the base, considering a clamped-free boundary condition, it is possible to obtain the expressions that relate the cross-section width and stress conditions with the acting forces *N* and *V,* normal and lateral forces, respectively. The lateral load V is explicitly incremented, the neutral axis position is evaluated at each step, and the displacement increment is then obtained, giving the next point of the *V* vs. *D* curve. It is interesting to notice that there are two possibilities for the stress state at the base of the structure: the whole cross-section is compressed $x_u \geq B$; part of the cross-section is compressed $x_u < B$. Therefore, for each situation (segment), $\varepsilon_{máx}$ (or $\sigma_{máx}$) must be calculated.

3.1 Entire cross-section is compressed (Segment 1)

From Fig 3, it is possible to obtain some relations between acting forces, bending moments, and strains as expressed in Equation (1):

$$
\begin{aligned}
F &= F_A + F_B \\
F_A &= \sigma_{\min} Bt = E\varepsilon_{\min} Bt \\
F_B &= \left(\sigma_{\max} - \sigma_{\min}\right)\frac{Bt}{2} = E\left(\varepsilon_{\max} - \varepsilon_{\min}\right)\frac{Bt}{2} \\
M &= \left(\sigma_{\max} - \sigma_{\min}\right)\frac{Bt}{2}\ \frac{B}{2} - \frac{B}{3}\ = E\left(\varepsilon_{\max} - \varepsilon_{\min}\right)\frac{B^2 t}{12}
\end{aligned}
\tag{1}
$$

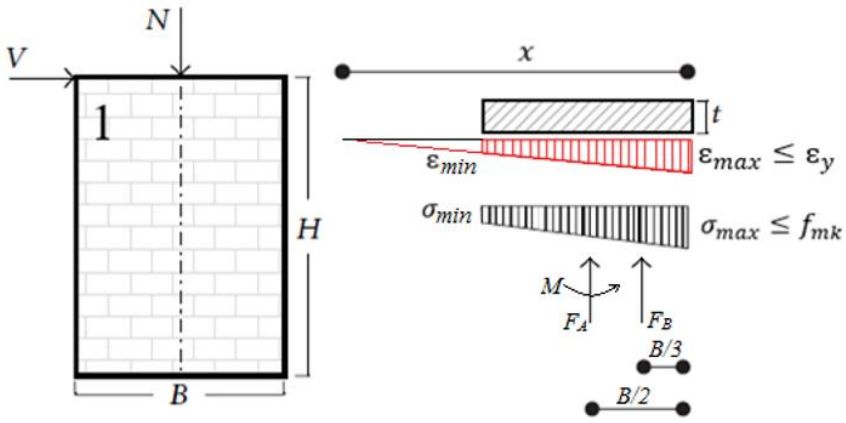

Figure 3 Masonry panel segment 1 characteristics (adapted from Grande et al., 2013).

For the case when x=B, which means ε_{min}=σ_{min}=0, the base of the panel is still under a compression-only state. Thus:

$$F_y \quad 0 \quad F \quad N \quad 0 \quad \sigma_{\max} \frac{Bt}{2} \quad N \quad 0 \quad \sigma_{\max} \quad \frac{2N}{Bt} \tag{2}$$
$$M \quad VH \quad \sigma_{\max} \frac{B^2 t}{12} \quad \frac{2N}{Bt} \frac{B^2 t}{12} \quad V \quad \frac{NB}{6H}$$

3.2 Part of the cross-section is compressed in the elastic regime (Segment 2)

As shown in Fig 4, imposing the equilibrium conditions, the following relations are obtained according to:

$$F = \sigma_{\max} \frac{xt}{2} = E\varepsilon_{\max} \frac{xt}{2} \tag{3}$$
$$M = \sigma_{\max} \frac{xt}{2} \left(\frac{B}{2} - \frac{x}{3} \right) = E\varepsilon_{\max} \frac{xt}{2} \left(\frac{B}{2} - \frac{x}{3} \right)$$

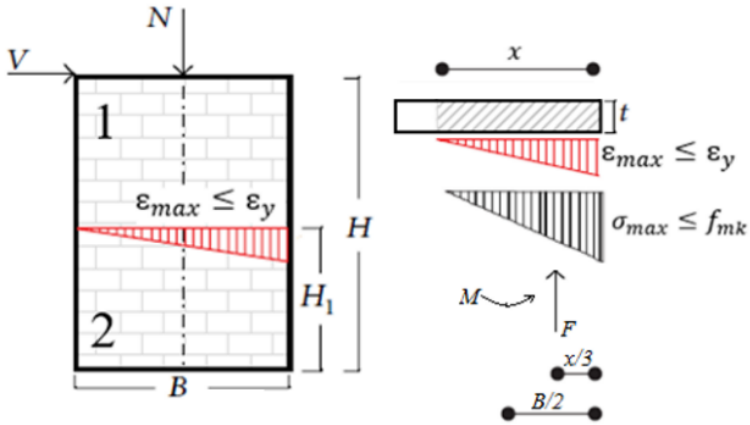

Figure 4 Masonry panel segment 2 characteristics (adapted from Grande et al., 2013).

For the limit case when $\sigma_{max} = f_{mk}$, the following value for V load is obtained:

$$f_{mk} \quad \frac{2N}{xt} \quad x \quad \frac{2N}{f_{mk} t} \tag{4}$$
$$M \quad VH \quad N \left(\frac{B}{2} - \frac{x}{3} \right) \quad N \left(\frac{B}{2} - \frac{2N}{3 f_{mk} t} \right) \quad V \quad \frac{N}{H} \left(\frac{B}{2} - \frac{2N}{3 f_{mk} t} \right)$$

The height H_1 can be calculated considering that at $(H - H_1)$ the situation is the same as when the panel starts to be tensioned, according to Equation (5):

$$V \quad \frac{NB}{6\left(H - H_1\right)} \quad H_1 \quad H \quad \frac{NB}{6V} \tag{5}$$

3.3 Part of the cross-section is compressed in the plastic regime (Segment 3)

From Fig. 5, after imposing the equilibrium conditions, the following relations are obtained according to Eq. (6).

$$\begin{aligned} F &= F_A + F_B \\ F_A &= f_{mk}\frac{x_s t}{2} \\ F_B &= f_{mk}\left(x - x_s\right)t \\ M &= F_A\ \frac{B}{2} - \ x - \frac{2x_s}{3}\ + F_B\ \frac{B}{2} - \frac{x - x_s}{2} \end{aligned} \tag{6}$$

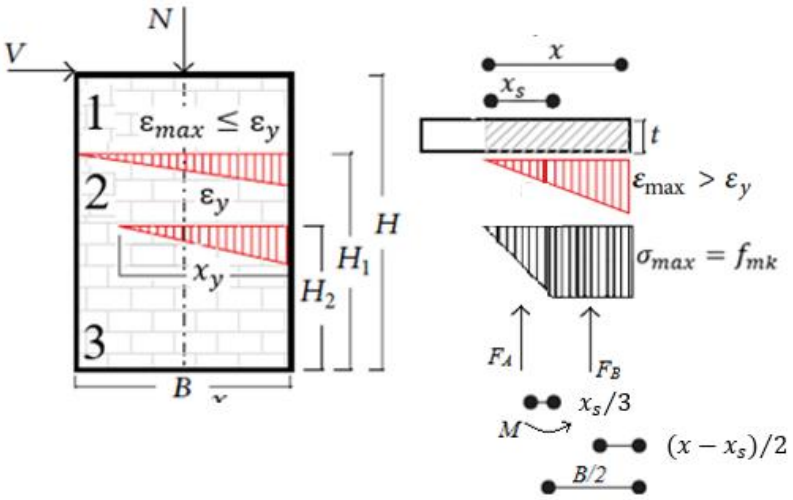

Figure 5 Masonry panel segment 3 characteristics (adapted from Grande et al., 2013).

The limit case happens when the panel is completely plasticized, in which there is no more possibility of equilibrium. This condition allows us to obtain the maximum value that load *V* can reach. The panel collapses when the ultimate load *V* is applied, or the ultimate strain ε_u is reached, whichever happens first. These conditions are shown in Equation (7).

$$\begin{aligned} &f_{mk} \quad \frac{N}{xt} \quad x \quad \frac{N}{f_{mk}t} \\ &M \quad VH \quad N\ \frac{B}{2}\ \frac{x}{2} \quad N\ \frac{B}{2}\ \frac{N}{2f_{mk}t} \quad V \quad \frac{N}{H}\ \frac{B}{2}\ \frac{N}{2f_{mk}t} \end{aligned} \tag{7}$$

The height H_2 can be calculated considering that at $(H - H_2)$ the situation is the same when the panel starts in the plastic regime, according to Equation (8):

$$V \quad \frac{N}{\left(H - H_2\right)}\ \frac{B}{2}\ \frac{2N}{3f_{mk}t} \quad H_2 \quad H \quad \frac{N}{V}\ \frac{B}{2}\ \frac{2N}{3f_{mk}t} \tag{8}$$

3.4 Finite element modeling

The finite element analysis developed in this work relies on the fact that each of the segments shown can be modeled using an element whose cross-section is based on the portion of the panel withstanding compression. Figure 6 shows each segment according to its stress state. Segment 1 is entirely under compression (marked in red) and can be modeled as a constant cross-section element with length given by ($H-H_1$). Segment 2 (marked in green) is compressed at the top, but its bottom is partially ruptured due to tension, so only the compressed portion of the cross-section is considered; its length is given by (H_1-H_2). For segment 3 (blue), a similar situation occurs, but in this case, the bottom is already experiencing plastic deformation. The portion of the panel marked in yellow does not contribute to the strength of the wall and is therefore neglected. The proposed methodology consists of determining the number of segments for a specific value of the lateral load V, considering all other parameters as constant (material and geometric characteristics, axial load N). After the number of segments is determined, the stress state (maximum and minimum stresses and strains), width, and length of each segment can be calculated according to Equations (1) to (8).

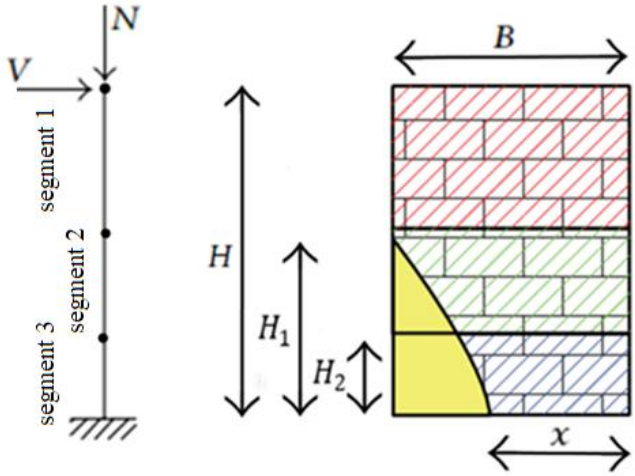

Figure 6 Masonry panel finite elements for each segment.

If constant cross-section finite elements are used, an accurate result can only be achieved if each segment is divided into several elements, i.e., if discretization is performed. In this work, one and 10 elements per segment were tested. On the other hand, if variable cross-section elements are employed, there is no need for discretization, and only one element per segment can be used.

4 FINITE ELEMENTS USED

Developed initially in Grande et al. (2013), the main approach adopted in this work is the use of a one-dimensional finite element analysis to obtain the nonlinear response of a masonry panel, namely its capacity curve. For this purpose, two types of finite element formulations were used in this paper: constant and variable cross-section finite elements. From the expressions in section 2, it is possible to obtain the stress state in any section of the panel for a specific lateral load *V*. According to the stress state, the panel can be divided into one, two, or three segments, each with its own behavior, as explained in section 2. For the segments in which tension exists, part of the cross-section is neglected, and therefore a variable width becomes present, as shown in Fig 6. These variable cross-section segments can be analyzed either by discretizing them into several constant cross-section finite elements (the usual approach) or by using a finite element whose stiffness coefficients were specifically obtained for dealing with variable cross-sections. In this case, there is no need for discretization.

4.1 Constant cross-section finite element (CS)

Easily found in the literature, this finite element is based on cubic (Hermitian) shape functions, which are calculated from infinitesimal element equilibrium in the undeformed configuration. In this approach, the geometric nonlinearity at an infinitesimal level is disregarded, and discretization (subdivision) of the analyzed region is required for reliable results. In this work, for the constant cross-sectional finite element, all numerical applications were discretized in one (CS1) and 10 elements (CS10). The CS1 approach is the one proposed by Grande et al. (2013). Fig 7 shows a convergence study

performed in one of the panels taken from the literature. For 10 or more elements, the relative change in the result becomes a straight line in the log-log plot, showing that the error and the element size follow a power-law relationship. For that reason, 10 was taken as the number of elements per segment used as the discretization pattern for constant cross-section elements.

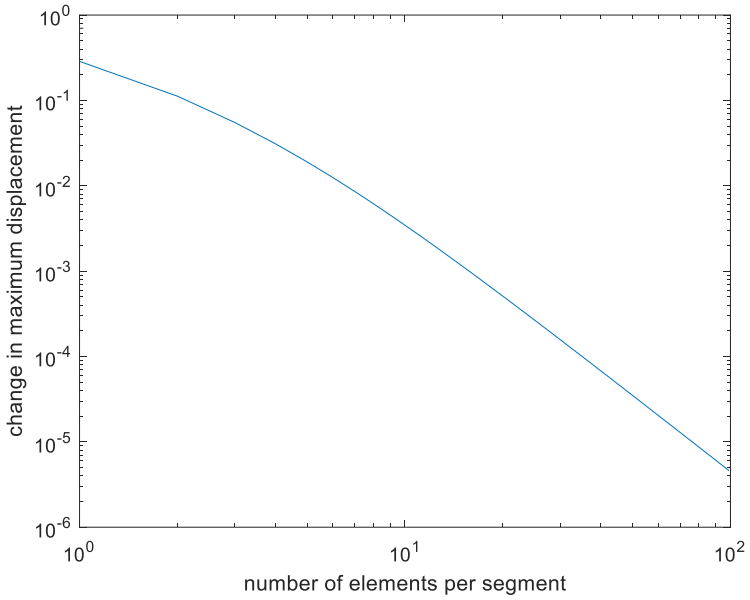

Figure 7 Convergence study for CS element.

Since the length/width ratio of shear walls is typically low, the shear deformation plays a preponderant role in the masonry panel analysis. Thus, Timoshenko's beam theory is employed, and the stiffness matrix of the constant cross-sectional finite element can be obtained using straightforward techniques for solving a fourth-order differential equation (typically Hermitian polynomials). The result is shown in Equation (9):

$$K = \begin{bmatrix} \frac{EA}{L} & 0 & 0 & -\frac{EA}{L} & 0 & 0 \\ 0 & \frac{12EI}{L^3}\frac{1}{1+12\Omega} & \frac{6EI}{L^2}\frac{1}{1+12\Omega} & 0 & -\frac{12EI}{L^3}\frac{1}{1+12\Omega} & \frac{6EI}{L^2}\frac{1}{1+12\Omega} \\ 0 & \frac{6EI}{L^2}\frac{1}{1+12\Omega} & \frac{4EI}{L}\frac{1+3\Omega}{1+12\Omega} & 0 & -\frac{6EI}{L^2}\frac{1}{1+12\Omega} & \frac{2EI}{L}\frac{1-6\Omega}{1+12\Omega} \\ -\frac{EA}{L} & 0 & 0 & \frac{EA}{L} & 0 & 0 \\ 0 & -\frac{12EI}{L^3}\frac{1}{1+12\Omega} & -\frac{6EI}{L^2}\frac{1}{1+12\Omega} & 0 & \frac{12EI}{L^3}\frac{1}{1+12\Omega} & -\frac{6EI}{L^2}\frac{1}{1+12\Omega} \\ 0 & \frac{6EI}{L^2}\frac{1}{1+12\Omega} & \frac{2EI}{L}\frac{1-6\Omega}{1+12\Omega} & 0 & -\frac{6EI}{L^2}\frac{1}{1+12\Omega} & \frac{4EI}{L}\frac{1+3\Omega}{1+12\Omega} \end{bmatrix} \quad (9)$$

$$A = Bt, \quad I = \frac{B^3 t}{12}, \quad \Omega = \frac{EI}{\chi G A L^2}$$

where L is the length of the element, G is the transverse modulus of elasticity, and χ=5/6 is the shear shape factor for a rectangular section.

Since constant cross-section elements are used to model variable-width segments of the panels, the criterion used in this study was to calculate the geometric properties (namely area and inertia) using the average width between top and bottom values. When using one element per segment, these widths are taken directly from the calculated neutral

axis values; when more than one element is used, there is a need to interpolate these values to obtain the characteristic widths for each subdivision.

4.2 Variable cross-section finite element (VS)

To reduce the discretization in finite element numerical modeling, the element with variable cross-section for each masonry panel segment is used, considering that the width B varies linearly along the element as shown in Fig 8. Therefore, *B* was written as a function of the known values of the beginning (B_0) and end ($B_1 = \alpha B_0$) of each element of length *L*.

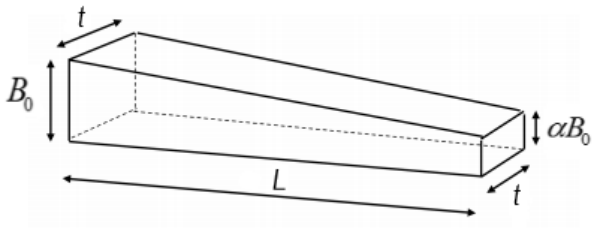

Figure 8 Variable cross-section element.

According to the following, the stiffness matrix of the variable cross-sectional element using Timoshenko's beam theory is:

$$K = \begin{bmatrix} k_1 & 0 & 0 & -k_1 & 0 & 0 \\ 0 & k_2 & k_3 & 0 & -k_2 & k_4 \\ 0 & k_3 & k_5 & 0 & -k_3 & k_6 \\ -k_1 & 0 & 0 & k_1 & 0 & 0 \\ 0 & -k_2 & -k_3 & 0 & k_2 & -k_4 \\ 0 & k_4 & k_6 & 0 & -k_4 & k_7 \end{bmatrix} \quad (10)$$

$$A_0 = B_0 t, \quad I_0 = \frac{{B_0}^3 t}{12}, \quad \Omega_0 = \frac{EI_0}{\chi G A_0 L^2}$$

5 NUMERICAL EXAMPLES

The following panels were modeled using three approaches: (1) one constant cross-section element per segment, named CS1, as proposed by Grande et al. (2013); (2) ten (10) constant cross-section elements per segment, named CS10, i.e., a more refined mesh using the same element proposed by Grande et al. (2013); (3) one variable cross-section element per segment, named VS. As mentioned in section 3.1, for constant cross-section elements, geometric properties were calculated using the average width value between top and bottom for each subdivision. Results were tested against experimental values from the references. Table 1 shows the parameters for these panels. For all panels, Poisson's ratio ν = 0.15 and ultimate strain ε_u = 0.1. The usual value for ultimate strain is lower than the one used, in this study the values were chosen as to force the collapse by flexure mechanism (total plastification).

Table 1 Parameters of the tested panels.

Ref. (Fig)	*B* (mm)	*H* (mm)	*t* (mm)	*E* (MPa)	f_{mk} (MPa)	*N* (kN)
Fantoni, 1981 (7a)	1250	1820	500	1118	6.0	343
Fantoni, 1981 (7b)	1250	1850	500	1290	3.7	358
Fantoni, 1981 (7c)	1250	1830	500	1125	6.0	355
Giambanco et al., 1996 (7d)	1200	2400	500	726	4.5	311
Giuffre and Grimaldi, 1985 (7e)	980	980	290	4880	3.4	242
Callerio, 1998 (7f)	1000	2000	250	1910	6.2	150

Some of the panels, namely references Fantoni (1981) and Callerio (1998), had different boundary conditions than clamped-free. Those tests were performed using a fixed rotation support on the top of the panel, allowing only lateral displacement but with no rotation. The same FEM model can be used for these boundary conditions, with the following adaptations: the panel is modeled using half the height, and the displacement measured at the top of this new panel should be doubled to account for the symmetry in the deformed configuration, as shown in Fig 9. To satisfy equilibrium, the moment reaction M at the top and bottom of the panel must be equal to VH/2. That value is the same as that obtained for a clamped-free element with half the length of the clamped-roller panel, as shown in the right part of the figure. This adaptation allows the use of the displacement at the top of the clamped-free half-length panel.

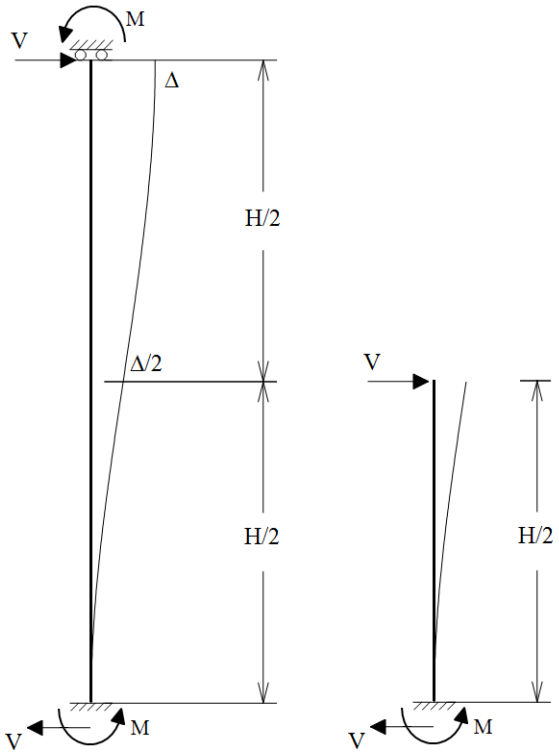

Figure 9 Clamped-roller boundary condition and the required adaptations.

It is clear from the curves in Fig 10 that the variable cross-section element provides good agreement with experimental values and reduces the need for discretization, allowing the use of only one finite element per segment, which is computationally less expensive and more intuitive. The agreement in terms of ultimate load is far more satisfactory than for ultimate displacement. That is due probably to experimental failure modes (diagonal shear and/or horizontal sliding), different from those modeled in this study. Another source of inaccuracy is the lack of proper management of the region in which plastic deformation occurs.

Table 2 shows the relative errors calculated in terms of ultimate loads and displacements for each panel and each of the studied approaches. In bold font is the average result for VS (variable cross-section elements), which presented the best performance.

Table 2 Parameters of the tested panels.

Ref. (Fig)	Experimental		Error CS1		Error CS10		Error VS (present)	
	V_u (kN)	D_u (mm)	Δ_V (%)	Δ_D (%)	Δ_V (%)	Δ_D (%)	Δ_V (%)	Δ_D (%)
Fantoni, 1981 (7a)	222.4	8.91	3.8	51.8	3.8	21.1	3.8	19.4
Fantoni, 1981 (7b)	190.6	5.98	7.2	45.2	7.2	30.4	7.2	30.0
Fantoni, 1981 (7c)	238.0	9.38	7.8	53.1	7.8	24.5	7.8	23.0
Giambanco et al., 1996 (7d)	65.0	21.66	5.9	37.8	5.9	5.2	5.9	6.9
Giuffre and Grimaldi, 1985 (7e)	83.8	1.28	8.3	55.5	8.3	50.9	8.3	50.8
Callerio, 1998 (7f)	75.9	12.67	10.8	86.9	10.8	77.6	10.8	54.2
Average	–	–	7.3	55.1	7.3	35.0	**7.3**	**30.7**

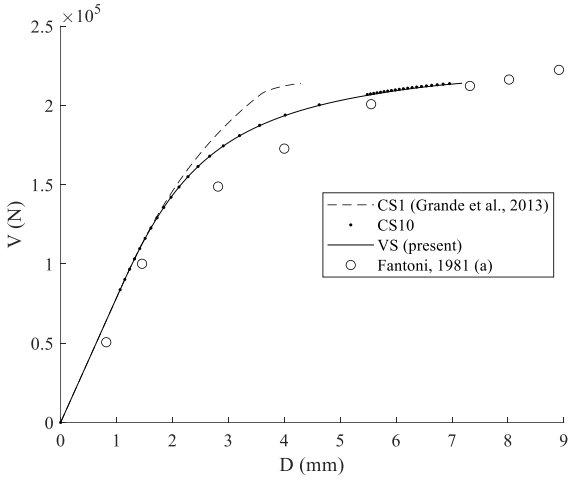

(a)

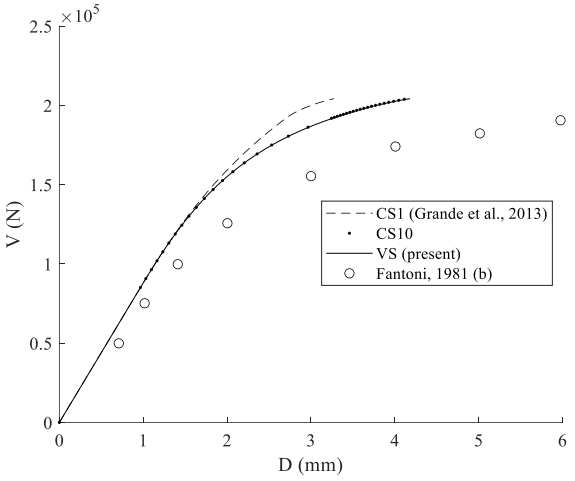

(b)

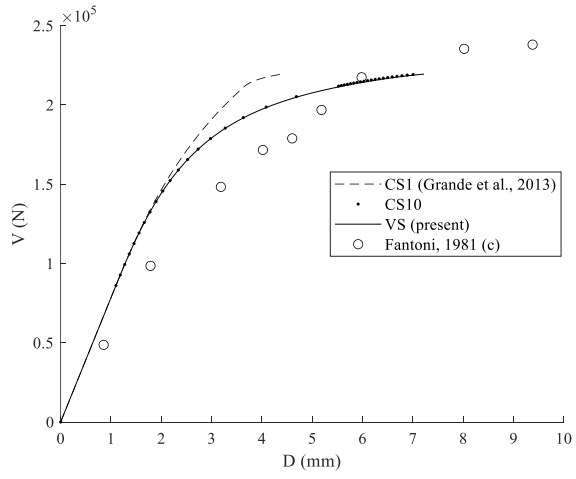

(c)

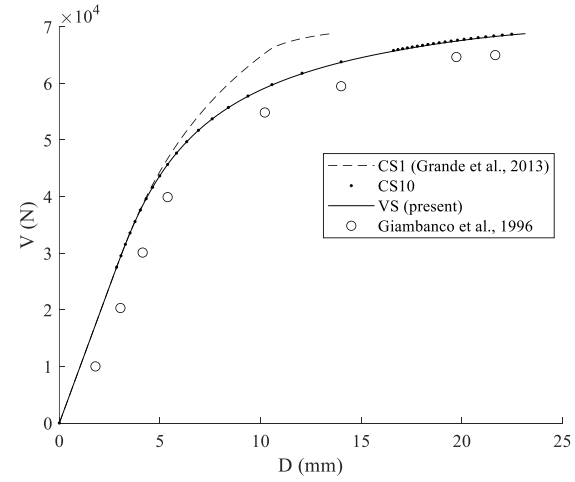

(d)

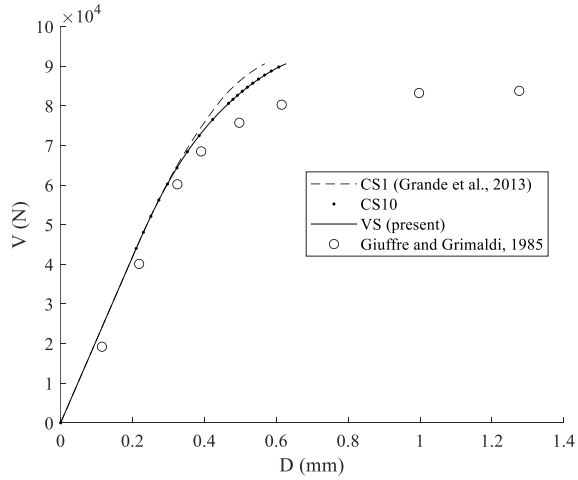

(e)

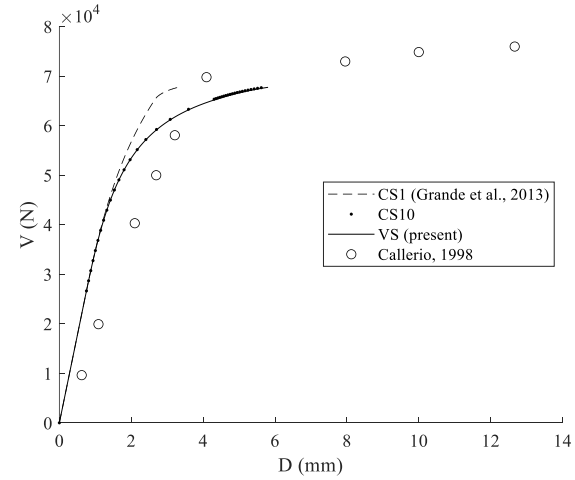

(f)

Figure 10 Results for load vs. lateral displacement.

4 CONCLUSIONS

This work investigates a simple approach to evaluate the nonlinear response of masonry shear walls based on a formulation that employs Timoshenko frame elements with constant and variable cross-sections. At each load increment, force and moment equilibrium relations are used to identify the current normal stress distribution along the cross-sections for each frame element, based on the no-tension assumption and an elastic–perfectly plastic behavior in compression. The geometrical and mechanical properties of each frame element are estimated from the cross-section portions under compression.

For the evaluation of load capacity curves, it was found that simulations that use frame elements with constant cross-sections to discretize a shear wall along its length provide accurate results only if relatively dense meshes are employed. On the other hand, in the case of elements with linearly varying cross-sections, only one element per segment is required to accurately represent the change, along the panel axis, of the section width that is under compression. The performed numerical simulations show that these proposed models are in good agreement with experimental results and may be employed to assess the load capacity of masonry shear walls in a pre-design phase. Considering the high complexity of the behavior of masonry panels (orthotropy, nonlinearity, modes of collapse), the results are satisfactory. Literature shows several sophisticated numerical models that are unable to accurately grasp the lateral load vs. displacement behavior of masonry panels, so this simple model can be considered a good contribution in the field.

Future works include: (i) the consideration of out-of-plane behavior, with the inclusion of distributed lateral load and the possibility of buckling; (ii) modeling of the panel's nonlinear behavior using plasticity theory; (iii) inclusion of reinforcement; (iv) modeling of the masonry material with tension strength value instead of no tension.

Author's Contributions: Conceptualization, RB Burgos and MFF Oliveira; Methodology, ASA Gesteira, MFF Oliveira and RB Burgos; Investigation, ASA Gesteira and LE Silva; Writing - original draft, MFF Oliveira and RB Burgos; Writing - review & editing, MFF Oliveira and RB Burgos; Funding acquisition, RB Burgos; Supervision, MFF Oliveira and RB Burgos; Validation, MFF Oliveira and LE Silva.

Data Availability: Research data is available in the body of the article

Editor: Marcílio Alves

References

Addessi, D, Mastrandrea, A, Sacco, E. An equilibrated macro-element for nonlinear analysis of masonry structures, Eng Struct., 2014;70: 82-93.

Addessi, D, Re, PD, Sacco, E. Micromechanical and multiscale computational modeling for stability analysis of masonry elements, Eng Struct., 2020;211: 110428.

Asikoglu, A, Vasconcelos, G, Lourenço, PB, Panto, B. Pushover analysis of unreinforced irregular masonry buildings: Lessons from different modeling approaches, Eng Struct., 2020;218: 110830.

Benedetti, A, Steli, E. Analytical models for shear–displacement curves of unreinforced and FRP reinforced masonry panels, Constr Build Mater., 2008;22(3): 175-185.

Callerio, A. Comportamento sismico delle murature ne-gli edifici monumentali: un metodo di analisi basato sulla meccanica del danneggiamento, Ph.D. thesis, University of Naples, 1998.

D'Altri, AM, Sarhosis, V, Milani, G, Cattari, S, Lagomarsino, S, Sacco, E, et al. Modeling strategies for the computational analysis of unreinforced masonry structures: review and classification, Arch Comput Methods Eng., 2020;27: 1153-1185.

Di Pasquale, S. New trends in the analysis of masonry structures, Meccanica, 1992;27(3): 173-184.

Fantoni, L. Rapporto Sulle Prove della Capacità Portante di Murature in Pietrame Iniettate, CRAD: Centro di Ricerca Applicata e Documentazione, Udine, Italy, 1981.

Galasco, A, Lagomarsino, S, Penna, A, Resemini, S. Non-linear seismic analysis of masonry structures, Proceedings of the 13th World Conference on Earthquake Engineering, Vancouver, 2004.

Gesteira, ASA, Burgos, RB, Oliveira, MFF. Lateral load behavior of masonry panels using frame elements with variable cross-section, Proceedings of XLI CILAMCE, November 2020.

Gesteira, ASA. Modeling of masonry panels subjected to lateral loading using frame finite elements with variable cross section, MS thesis (in Portuguese), PGECIV, UERJ, Rio de Janeiro, RJ, Brazil, 2021. http://www.pgeciv.uerj.br/dissertacoes/

Giambanco, G, Rizzo, S, Spallino, R. Il Modello di Interfaccia a Doppia Asperità per l'analisi delle Strutture Discontinue, Atti del Convegno Nazionale: La Meccanica delle Murature tra Teoria e Progetto, Messina, Italy, 1996.

Giuffre, A, Grimaldi, A. Studi Italiani Sulla Meccanica delle Murature, Atti del Convegno: Stato dell'arte in Italia sulla Meccanica delle Murature, Roma, Italy, 1985.

Grande, E, Maura, I, Rasulo, A, Sacco, E. A frame element model for the nonlinear analysis of FRP strengthened masonry panels subjected to in-plane loads, Adv Mater Sci Eng., 2013: 754162.

Gürel, MA, Kısa, M, Çili, FMA. Lateral stiffness of unreinforced masonry circular columns under cracked conditions, Turkish J Eng Environ Sci., 2006;30: 57-68.

Gurel, MA, Pekgokgoz, RK, Çili, FMA. Strength capacity of unreinforced masonry cylindrical columns under seismic transverse forces, Bull Earthquake Eng., 2012;10: 587–613.

Heyman, J. The stone skeleton, Int J Solids Struct., 1966; 2(2): 249-279.

Lagomarsino, S, Penna, A, Galasco, A, Cattari, S. TREMURI program: an equivalent frame model for the nonlinear seismic analysis of masonry buildings, Eng Struct.¸2013;56: 1787-1799.

Liberatore, D, Addessi, D. Strength domains and return algorithm for the lumped plasticity equivalent frame model of masonry structures, Eng Struct., 2015;91: 167-181.

Lourenço, PB. Computational strategies for masonry structures: multi-scale modelling, dynamics, engineering applications and other challenges, Proceedings of the SEMNI 2013, Bilbao, Spain, 2013.

Lu, M, Schultz, A, Stolarski, A. Application of the arc-length method for the stability analysis of solid unreinforced masonry walls under lateral loads, Eng Struct., 2005;27: 909-919.

Magenes, G, Calvi, GM. In-plane seismic response of brick masonry walls, Earthquake Eng Struct Dyn., 1997;26(11): 1091-1112.

Math Works, Inc. MATLAB. Version 9.4.0.857798 (R2018a), 2018. Computer Software.

Mura. I. Stability of nonlinear masonry members under combined load, Comp & Struct., 2008;86: 1579-1593.

Pasticier, L, Amadio, C, Fragiacomo, M. Non-linear seismic analysis and vulnerability evaluation of a masonry building by means of the SAP2000 V.10 code, Earthquake Eng Struct Dyn., 2008;37: 467-485.

Penna, A, Galasco, A, Magenes, G. Macro-element modelling of earthquake-induced local failure modes in existing masonry building, Proceedings of SECED 2015 Conference, Cambridge, UK, 2015.

Penna, A, Lagomarsino, S, Galasco, A. A nonlinear macroelement model for the seismic analysis of masonry buildings, Earthquake Eng Struct Dyn., 2014;43: 159-179.

Petrovcic, S, Kilar, V. Seismic failure mode interaction for the equivalent frame modeling of unreinforced masonry structures, Eng Struct., 2013;54: 9-22.

Raka, E, Spacone, E, Sepe, V, Camata, G. Advanced frame element for seismic analysis of masonry structures: model formulation and validation, Earthquake Eng Struct Dyn., 2015;44: 2489-2506.

Roca, P, Cervera, M, Gariup, G, Pela, L. Structural analysis of masonry historical constructions. Classical and advanced approaches, Arch Comput Methods Eng, 2010;17: 299-325.

Roca, P, Molins, C, Marí, AR, Asce, M. Strength capacity of masonry wall structures by the equivalent frame method, J Struct Eng., 2005;131(10): 1601-1610.

Roca, P. Assessment of masonry shear-walls by simple equilibrium models, Constr Build Mater., 2006;20(4): 229-238.

Sabatino, R, Rizzano, G. Nonlinear static analysis of masonry structures. Simplified equivalent frames and accurate models, Proceeding of the 14th ECEE, Ohrid, 2010.

Salmanpour, AH, Mojsilovic, N, Schwartz, J. Deformation capacity of unreinforced masonry walls subjected to in-plane loading: a state-of-art review, Int J Adv Struct Eng., 2013;5(22): 1-12.

Salonikios, T, Karakostas, C, Lekidis, V, Anthoine, A. Comparative inelastic pushover analysis of masonry frames, Eng Struct., 2003;25: 1515-1523.

Simões, A, Milosevic, J, Meireles, H, Bento, R, Cattari, S, Lagormasino, S. Fragility curves for old masonry building types in Lisbon, Bull. Earthquake Eng., 2015;13: 3083-3105.